Computational Approaches to Activity in Rhodium-Catalysed Hydroformylation

Dieter Gleich* and Jürg Hutter*[a]

Abstract: In this theoretical study on rhodium-catalysed hydroformylation we examine an unmodified hydridorhodium(I) carbonyl system **a** together with three variants modified by the model phosphane ligands PF_3 (system **b**), PH_3 (system **c**) and PMe_3 (system **d**), which show increasing basicity on the Tolman χ parameter scale. The olefinic substrate for all systems is ethene. Based on the dissociative hydroformylation mechanism, static and dynamic quantum-mechanical approaches are made for preequilibria and the whole catalytic cycle. Agreement with experimental results was achieved with regard to the predominance of phosphane monocoordination in systems **b**–**d**, different sensitivity of unmodified and modified systems towards hydrogen pressure and the early location of the rate-determining step. Neither the catalytic cycle as a whole nor olefin insertion as an important selectivity-determining step gives a clear picture of activity differences among **a**–**d**. However, the crucial first catalytic step, association of ethene to the active species $[HRhL_3]$ (L = CO, PR_3), may play the key role in the experimentally observed higher activity of **a** and systems with less basic phosphane ligands modelled by **b**.

Keywords: density functional calculations · hydroformylation · molecular dynamics · reaction mechanisms · rhodium

1. Introduction

With a capcity of more than six million tons per year, hydroformylation is one of the largest scale homogeneously catalysed industrial processes. Hydridorhodium(I) carbonyl complexes modified with ligands L such as phosphanes or phosphites are predominantly used (Scheme 1).[1]

Unmodified catalysts (L = CO) have the highest activity but low selectivities.[1b] As a rule of thumb, phosphane-modified systems give a faster turnover if the ligands are less "basic", that is, less electron-donating. Examples are alkylphosphanes or arylphosphanes bearing electron-withdrawing substituents.[2] However, as late as 1995, the manifold ligands and reaction parameters led to the conclusion that "the overall activity of phosphane-modified catalysts remains completely unpredictable".[1b]

Thanks to enormous progress in methods of computational chemistry in the field of transition metal catalysed reactions,[3] since 1997 many theoretical studies on hydroformylation have been published, some of which also deal with issues of regioselectivity or stereoselectivity.[4–9] Apart from a kinetic model including a semiquantitative structure–activity relationship for chelating phosphite ligands,[10] the common theoretical approach for gaining information on activity has been to calculate energy profiles of molecular reactions. Schmid et al. treated some hydroformylation preequilibria with the model ligands PH_3 and PMe_3 using ab initio and DFT methods.[11] In the same year, the first calculation of the whole catalytic cycle (ligand PH_3, substrate ethene) at an ab initio level was reported by Morokuma et al.[12] Calculations with the hybrid density functional B3LYP[13–15] were recently reported for systems containing PH_3,[16,17a] monophosphane ligands with various alkyl and

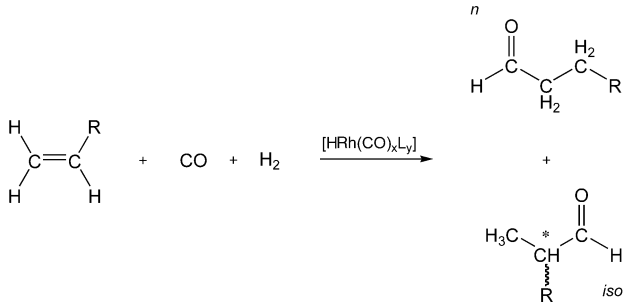

Scheme 1. Hydroformylation of a terminal olefin. The chirality center disappears for propene (R = Me), as do the *n* and *iso* regioisomers for ethene.

[a] Dr. D. Gleich, Prof. Dr. J. Hutter
Physikalisch-Chemisches Institut
Universität Zürich
Winterthurerstrasse 190
8057 Zürich (Switzerland)
Fax: (+41) 1-6356838
E-mail: hutter@pci.unizh.ch

Supporting information for this article is available on the WWW under http://www.chemeurj.org/ or from the author.

 DOI: 10.1002/chem.200305179 © 2004 Wiley-VCH Verlag GmbH & Co. KGaA, Weinheim

phenyl substituents[17b] and even a bis-phosphane chelate of real size.[18] In the last two cases, a two-layered ONIUM coupling scheme[19] was applied which fails if activity differences are caused by subtle electronic effects in the outer layer (e.g., substituents of phenyl rings connected to phosphorus atoms).[20]

So far, only parts of the catalytic cycle with an unmodified rhodium system have been investigated by means of quantum-mechanical methods.[8,21] Comparisons of different ligands were also confined to a single step.[17b] With the aim of obtaining a more profound theoretical understanding of the essential factors that govern hydroformylation activity, we examine in the present work the whole catalytic cycle for systems **a**–**d** at DFT and coupled cluster theory[22] (CCSD(T) variant) levels. The CCSD(T) single-point calculations on DFT-optimised geometries can supply accurate energy estimates for transition metal complexes.[3,11] System **a** is the unmodified type, while the other three systems are modified by model monophosphane ligands with increasing basicity on the χ parameter scale of Tolman:[23] PF_3 ($\chi = 18.3$, system **b**), PH_3 ($\chi = 8.3$, system **c**) and PMe_3 ($\chi = 2.0$, system **d**). Although ligand donor/acceptor properties deserve a quantitative treatment and depend on the specific reference complex,[24] the Tolman scale seems to give meaningful correlations for hydridorhodium(I) phosphane complexes.[16b,25] Moreover, **d** has more steric strain than **c**, **b** or **a**, that is, steric effects are also considered. The olefinic substrate for all systems is ethene. Static calculations are supplemented with dynamic calculations, namely, Car–Parrinello molecular dynamics (CPMD) simulations,[26] which have proven to be a vigorous tool for understanding time-dependent processes on a quantum-mechanical level.[26b] Some experience with reactions catalysed by rhodium and its neighbours ruthenium and palladium has already been gathered.[27–31]

2. Methods of Calculation

2.1. Static calculations with Gaussian 98:[32] DZVP and TZVP basis sets of Godbout et al.[33] were used for the elements H, C, O, F and P, while Rh was described by the small-core quasirelativistic effective core potential of Christiansen et al. and a double-zeta valence basis (abbreviated CE).[34]

Geometry optimisations with default values for grid and convergence parameters were carried out with the functional BP86.[13,35] DZVP(CE)- and TZVP(CE)-optimised structures had in almost all cases quasicongruent geometries.[36] All structures were verified to be true minima or first-order transition states by analytical determination of harmonic frequencies. CCSD(T)/TZVP(CE)//BP86/TZVP(CE) (abbreviated notation: CCSD(T)//BP86) single-point energy calculations were also carried out.

2.2. Static and dynamic calculations with CPMD:[37] Relativistic dual-space pseudopotentials of Hartwigsen et al. were used for all elements (large core on rhodium, abbreviation HGH).[38] General settings were applied to the following parameters: cell size (simple cubic, 14 Å), energy cutoff (70 Ry), electron mass (1000 a.u.) and time step (5 a.u. $\approx$ 0.12 fs). To test the correspondence between localised and plane-wave basis sets, geometry optimisations with default values for convergence parameters were made with the functional BP86. In most cases there was a close similarity to energies as well as geometries of TZVP(CE)-optimised structures.[36] Reaction pathways were searched for by "dynamic relaxation" of the transition states: A critical distance in each transition-state structure optimised at the BP86/DZVP(CE) level (Gaussian 98, cf. above) was allowed to shrink or grow during simulations at $T = 350$ K (Nosé–Hoover thermostatisation[39] with a coupling frequency of 2000 cm^{-1}). This method does not exactly correspond to the "dynamic reaction path" procedure at $T \approx 0$ K (NVE conditions),[40] but test calculations on our systems at increasing temperatures significantly shortened the simulation time without changing the results.

3. Results and Discussion

3.1. Mechanistic alternatives: The general course of rhodium-catalysed hydroformylation was proposed by Wilkinson et al.[41] They assumed a common mechanism which corresponds to the Heck–Breslow mechanism of the cobalt-catalysed reaction.[42] The mechanisms of unmodified and ligand-modified systems are assumed to be identical, too.

For system **a** a common catalyst precursor is $[Rh_4(CO)_{12}]$, which fragments under hydroformylation conditions into mononuclear species.[43] For modification with monophosphanes PR_3, mononuclear precursors such as $[Rh(acac)(CO)(PR_3)]$ and $[RhH(CO)(PR_3)_3]$ are converted to the experimentally observable dicarbonyl complex $[RhH(CO)_2(PR_3)_2]$.[2] As a consequence of the in situ preparation under a CO/H_2 atmosphere one always obtains a fraction of unmodified species that is diminished by an excess of phosphane ligand. In general, pentacoordinate complexes $HRhL_4$ **1** open the connection to the catalytically active species H-⟨Rh⟩.

3.1.1. Dissociative pathway: Dissociation of one ligand L (CO/PR_3) from **1** yields the active species **2**; 16- and 18-electron species alternate with each other during catalysis (Sche-

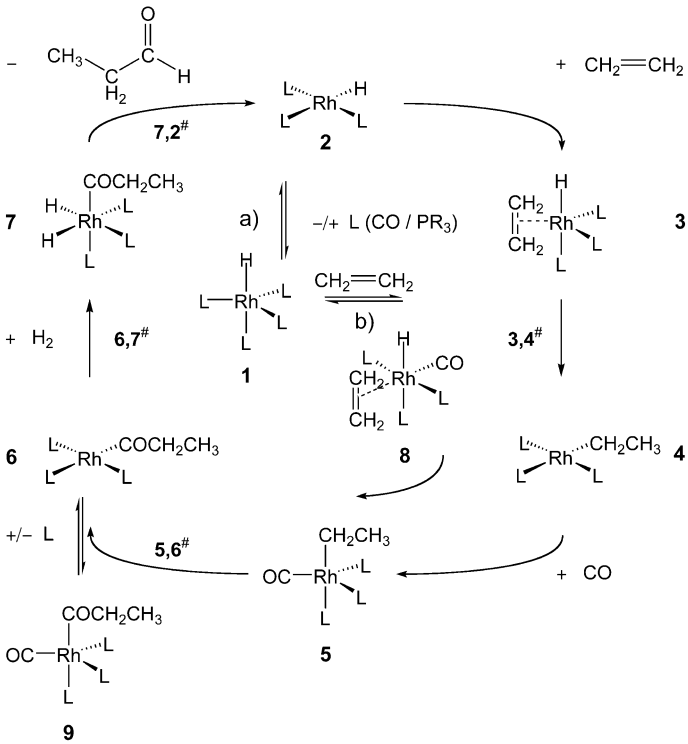

Scheme 2. a) Dissociative pathway. b) Associative pathway.

© 2004 Wiley-VCH Verlag GmbH & Co. KGaA, Weinheim

me 2a). The subsequent steps are olefin association **2**→**3**, olefin insertion **3**→**4**, CO association **4**→**5**, CO insertion **5**→**6**, oxidative hydrogen addition **6**→**7**, and reductive aldehyde elimination **7**→**2**.

3.1.2. Associative pathway: The associative pathway starts with olefin coordination to **1** and subsequent insertion without ligand dissociation, that is, the hydroformylation cycle up to complex **6** involves 18- and 20-electron species (Scheme 2b). This alternative dates back to a tentative explanation of Wilkinson et al. for differences in regioselectivities in hydrogenation und hydroformylation.[41b] An argument against the associative pathway is that neither a stable adduct **8** nor a transition state **8,5** could be found by geometry optimisations at the BP86/DZVP(CE) and B3LYP/DZVP(CE) levels, which supports the 18-electron rule.[44] Olefin association to **1** is also questioned by the fact that CO dissociation from chelate-coordinated **1** is very fast and clearly obeys a first-order rate law.[45] Since the dissociative pathway moreover uncontradictably fits newer experimental data[46] it was chosen for all calculations in this work.

3.2. Preequilibria

*3.2.1. System **a***: The last preequilibrium for **a** is the CO dissociation $[HRh(CO)_4]$ (**1-CO**)→$[HRh(CO)_3]$ (**2-CO**) + CO (Scheme 2a). $[HRh(CO)_4]$ was recently observed under experimental hydroformylation conditions[43] after its trigonal-bipyramidal C_{3v}-symmetrical structure had been predicted by theoretical calculations.[21]

The reaction **1-CO**→**2-CO** + CO was found to be endothermic (+115.8 kJ mol^{-1}) according to second-order Møller–Plesset (MP2)[47] geometry optimisations.[3,21] At the BP86/TZVP(CE) and CCSD(T)//BP86 levels, one obtains +88.1 and +86.6 kJ mol^{-1}, respectively. A similar excellent agreement between BP86 and CCSD(T) results was achieved for CO dissociation from PH_3-modified systems.[11]

*3.2.2. Systems **b–d***: As a consequence of phosphane modification, several interconversions of isomers of **1** augment the possible dissociation reactions. Thermochemical data of the most relevant,[46] namely, **1-(PR$_3$)$_2$-*ae*/*ee***→**2-(PR$_3$)$_2$-*ct*/*cc*/2-PR$_3$-*t*/*c*** + CO/PR$_3$,[48] are listed in Scheme 3.

All CO dissociation energies are higher than for **a**. For **2-(PR$_3$)$_2$-*cc*** there seems to be a correlation between Tolman basicity and CO dissociation energy, but the values are nearly constant in the case of **2-(PR$_3$)$_2$-*ct***.

Phosphane dissociation is easier than its CO counterpart. The highest value (**2-PMe$_3$-*t***) coincides with that of the CO dissociation of **a** (see above). If one compares **2-PR$_3$-*t*** with **2-PR$_3$-*c*** the energies for R = F (system **b**) and R = Me (system **d**) take on reverse values, while for R = H (system **c**) there is almost no change. **2-PH$_3$** is thus stabilised versus **2-(PH$_3$)$_2$** by about −50 kJ mol^{-1}. System **b** prefers **2-PF$_3$** by at least −35.3 kJ mol^{-1} (**2-PF$_3$-*c*/*t***) versus **2-(PF$_3$)$_2$-*cc***), but for **d** the differences shrink to −18.4 kJ mol^{-1} (**2-PMe$_3$-*c*** versus **2-(PMe$_3$)$_2$-*cc***) and −8.3 kJ mol^{-1} (**2-PMe$_3$-*t*** versus **2-(PMe$_3$)$_2$-*cc***), respectively.

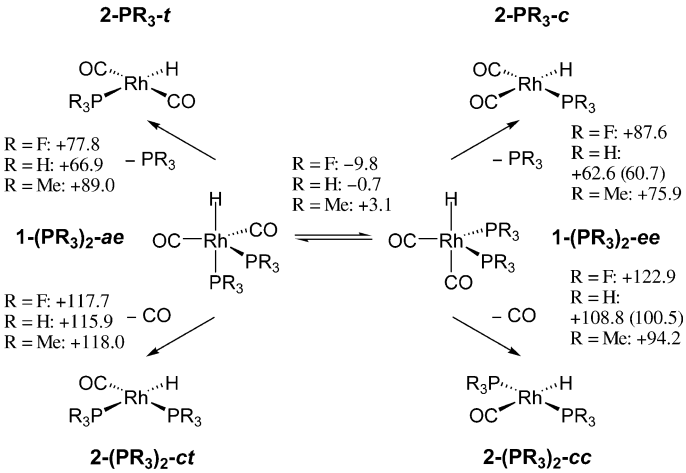

Scheme 3. Ligand dissociation reactions **1-(PR$_3$)$_2$-*ae*/*ee***→**2-(PR$_3$)$_2$-*ct*/*cc*/2-PR$_3$-*t*/*c*** + CO/PR$_3$ for systems **b–d**. Energies [kJ mol^{-1}] were calculated at the BP86/TZVP(CE) level; values in parentheses were taken from ref. [11].

3.2.3. Relation to experimental observations: The endothermicity of reactions **1**→**2** is overcome by the experimental temperature/pressure conditions and the exothermicity of the first catalytic steps (see Section 3.3.2).

At the BP86/TZVP(CE) level, the destabilisation of **2-PF$_3$**/**2-PH$_3$** versus **2-CO** is +37.7 kJ mol^{-1}/+30.0 kJ mol^{-1} at best, whereas **2-PMe$_3$** is stabilised versus **2-CO** by up to −13.2 kJ mol^{-1}. Hence the preequilibrium **1**→**2** + CO/PR$_3$ should be easily influenced by CO pressure and/or phosphane concentration, as is known from experiment.

For phosphane-modified systems, our calculations as well as mechanistic studies (ligand = PPh_3, substrate = ethene)[46] corroborate the dominance of phosphane monocoordination. We therefore based the comparison of systems **b**, **c** and **d** on **2-PR$_3$** and considered **2-(PR$_3$)$_2$** only for R = H in detail (system **c′**, see Section 3.3.2).

CO dissociation from **1** is likely to be orders of magnitudes faster than the hydroformylation reaction.[45,46] A similar situation should be valid for phosphane dissociation.[46] Hence, activity differences among systems **a–d** are expected to emerge during the catalytic cycle.

3.3. Catalytic cycle: The energy profiles of the dissociative pathway depicted in Scheme 2 were ascertained in two stages.

3.3.1. Selection of isomers: Since after phosphane modification each of the species in Scheme 2 exists as various isomers, one must find the more stable ones and connect them by suitable reaction pathways. Figure 1 shows selected isomers.

Early calculations showed that equatorial olefin coordination is strongly preferred in **3**.[49] Hydrogen addition **6**→**7** can proceed along two bond axes;[50] the isomers **7-PR$_3$-*e*/7-(PH$_3$)$_2$-*ae*** in Figure 1 are the most stable.[16b]

Reaction barriers of the CO association reaction **4**→**5** are neglected, since for a similar complex a value that was always zero was calculated.[51] First of all, barriers of the olefin association **2**→**3** are assumed to be negligible, too

 © 2004 Wiley-VCH Verlag GmbH & Co. KGaA, Weinheim

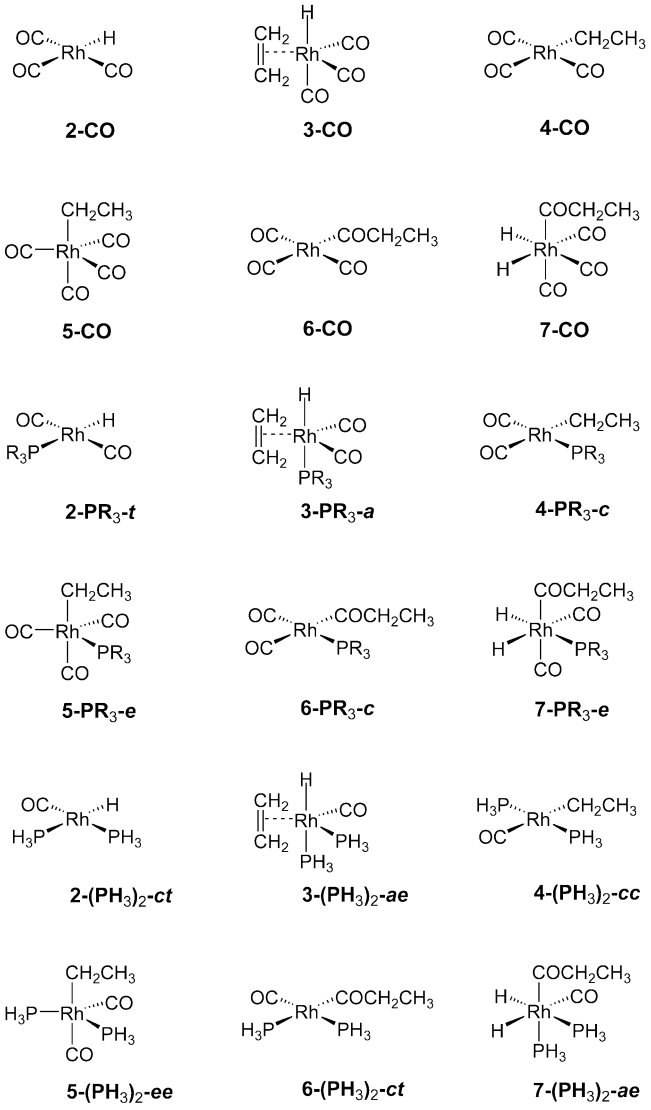

Figure 1. Selected isomers for the catalytic cycle with no (system **a**), one [R = F, H, Me (systems **b**, **c**, and **d**)] or two (system **c′**) phosphane ligands. Due to the schematic representation, isomers **6A** are omitted in favour of the identically coordinated complexes **7**.

(see Section 3.4.2). Energetically favoured isomers of the remaining transition states **3,4**, **5,6**, **6,7** and **7,2** were selected in agreement with former calculations (see Supporting Information).[5,17a] In most cases their dynamic relaxations towards starting materials/products started within the first 0.1 ps and gave identical isomers for systems **b**, **c** and **d** after a maximum simulation time of 0.6 ps. Ethene insertion resulted for both **3-PR$_3$-*a*** and **3-PR$_3$-*e*** (the latter isomer is not shown in Figure 1) in **4-PR$_3$-*c***, whereas **3-(PR$_3$)$_2$-*ae*** was connected with **4-(PR$_3$)$_2$-*cc***, and **3-(PR$_3$)$_2$-*ee*** (not shown in Figure 1) with **4-(PR$_3$)$_2$-*ct*** (not shown in Figure 1). The CO insertion pathway for system **c′**, **5-(PH$_3$)$_2$-*ee*** → **5,6-(PH$_3$)$_2$-*ee***, led, in contrast to former results,[17a] not to the *cis–cis* but to the *cis–trans* complex **6-(PH$_3$)$_2$-*ct***, which consequently changed the isomer distribution of the following steps. Backward dynamic relaxations of **6,7** always proceeded via nonclassical dihydrogen complexes[52,53] **6A**, which sometimes dissociated during the run. Forward dynamic relaxations of **7,2** never led to formation of an adduct between **2** and propionaldehyde, as has been suggested previously.[12]

The pathways were combined to give the same isomer of **2** at the beginning and end of the catalytic cycle. Consequently, **2-PR$_3$-*t*** and **2-(PH$_3$)$_2$-*ct*** were chosen although they are moderately higher in energy than **2-PR$_3$-*c*** and **2-(PH$_3$)$_2$-*cc*** (not shown in Figure 1, see Section 3.4.2). Note that after olefin insertion both pathways from **2-PR$_3$-*c*/*t*** merge in **4-PR$_3$-*c*** (cf. above).

3.3.2. Reaction profiles with energy corrections: In this section, reaction profiles of all systems on the BP86/TZVP(CE) level are discussed with a) no, b) zero-point and c) free-energy ($T = 298.15$ K) corrections. If not mentioned explicitly, energies can be found in Table 1 and Figures 2 and 3.

For the hydroformylation sum reaction, the energy differences between intermediate **2** at the beginning and at the end of the cycle correspond to the values of the hydroformylation sum reaction (see last row of Table 1). After zero-point correction, agreement with the experimental enthalpy value of $-125\ \mathrm{kJ\,mol^{-1}}$ is sufficient.[1a] Since the number of particles changes during the sum reaction from three to one, the energy value is more than halved after free-energy correction.

For system **a** the associations **2**→**3/4**→**5** are far more exothermic (2/3 of the sum reaction energy) than the insertions **3**→**4/5**→**6**. Reductive elimination **7**→**2** has even lower exothermicity, followed by dihydrogen addition **6A**→**7**, which is almost thermoneutral, whereas dihydrogen association **6**→**6A** is clearly endothermic.

Beginning with the lowest barrier value, the ranking of the four calculated transition states is **6A,7** ($18.5\ \mathrm{kJ\,mol^{-1}}$) ≪ < **7,2** ($34.6\ \mathrm{kJ\,mol^{-1}}$) ≪ **3,4** ($46.9\ \mathrm{kJ\,mol^{-1}}$) ≈ **5,6** ($51.0\ \mathrm{kJ\,mol^{-1}}$).[54] If one does not consider **6A**, the barrier of **6**→**7** comes very close to that of **7**→**2** (33.1 versus $34.6\ \mathrm{kJ\,mol^{-1}}$).

Figure 3 compares BP86 and CCSD(T) energies. Up to CO insertion transition state **5,6**, agreement between the two profiles is acceptable. Intermediate **6** alters this situation: Whereas **5**→**6** is predicted to be exothermic by BP86, the CCSD(T) profile is endothermic. This discrepancy has also been reported for a system with PH_3 ligands.[17a] Transitions **6**→**7** and **7**→**2** have inverted CCSD(T) thermochemistries, too, and the value for the sum reaction differs by about $-35\ \mathrm{kJ\,mol^{-1}}$. The CCSD(T) barriers are, with exception of **6A,7**, up to $24.5\ \mathrm{kJ\,mol^{-1}}$ (**5,6**) higher than the BP86 barriers. The graduation is more distinct, but the energetic ranking is essentially identical: **6A,7** ≪ < **7,2** < **3,4** ≪ **5,6**. The discrepancies between BP86 and CCSD(T) energies may be due to the different dependence of the methods on basis set superposition errors.[55]

After zero-point correction, the exothermicities are reduced by up to $10.6\ \mathrm{kJ\,mol^{-1}}$ (**2**→**3**), the same value by which the endothermicity of **6**→**6A** is raised. The transition-state ranking hardly changes (**6A,7** ≪ < **7,2** ≪ **3,4** < **5,6**). After omission of **6A**, however, the barrier of **6**→**7** becomes almost identical with that of **3**→**4** (40.8 versus $41.5\ \mathrm{kJ\,mol^{-1}}$).

© 2004 Wiley-VCH Verlag GmbH & Co. KGaA, Weinheim

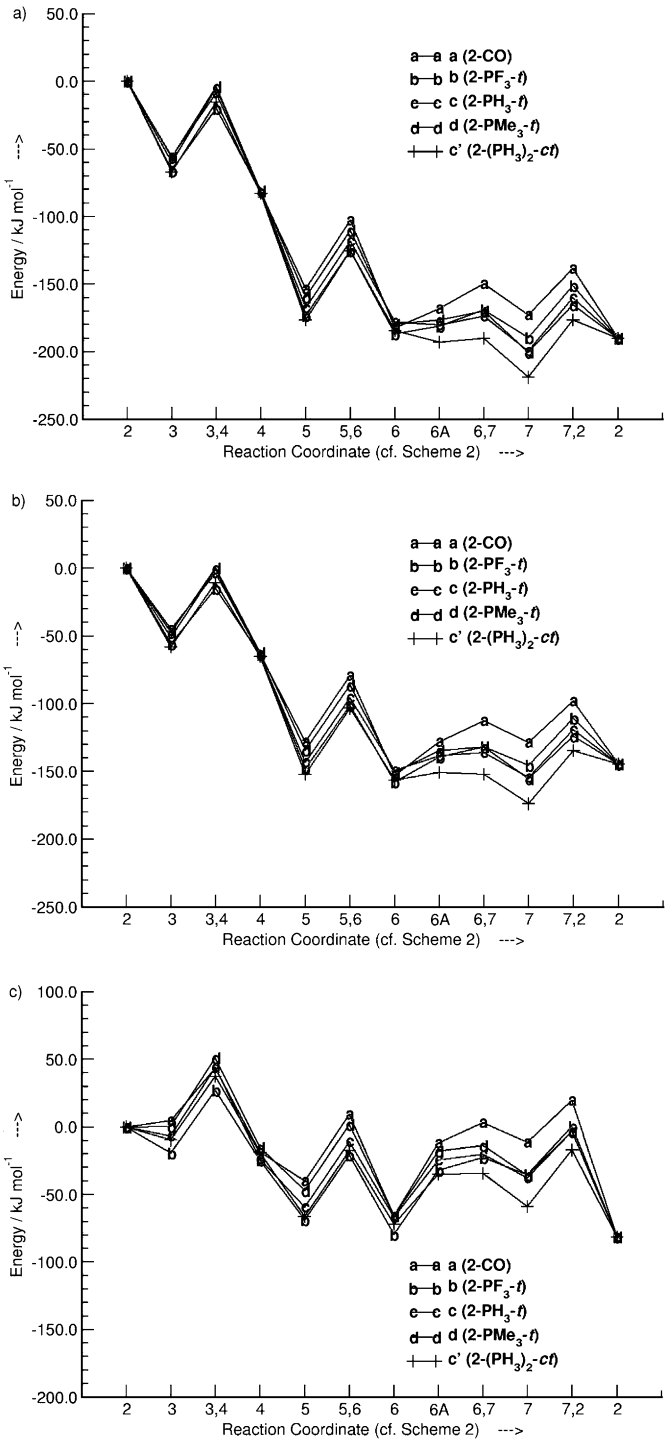

Figure 2. Reaction profiles of all systems at the BP86/TZVP(CE) level with a) no, b) zero-point and c) free-energy corrections (T = 298.15 K).

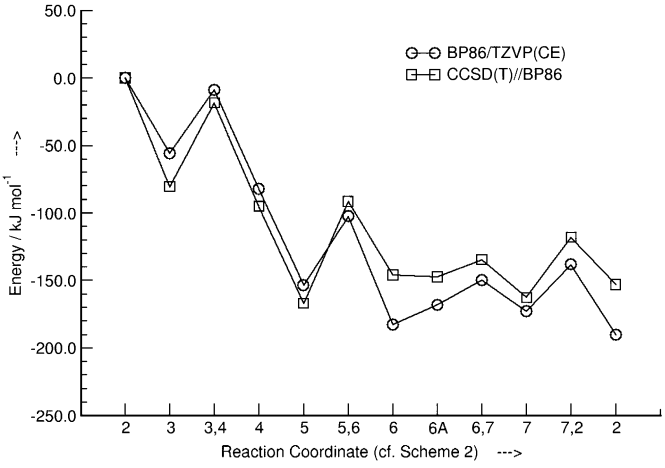

Figure 3. Reaction profiles of system **a** at the BP86/TZVP(CE) and CCSD(T)//BP86 levels without energy correction.

As expected, the free-energy correction chiefly affects all steps with significant entropic contributions, that is, **2**→**3**, **4**→**5**, **6**→**6A**, **6**→**7** and **7**→**2**. Step **7**→**2** is now the most exergonic reaction, **2**→**3** is weakly endergonic (see Section 3.4.2) and **6**→**6A** shows a strong increase of + 39.6 kJ mol^{-1}. If one neglects **6A**, the barrier of **6**→**7** becomes the highest in the catalytic cycle (68.9 kJ mol^{-1}), followed by that of **5**→**6** (49.2 kJ mol^{-1}).

For systems **b**–**d** (phosphane monocoordination), the most obvious divergence from system **a** stems from **6**→**7** and **7**→**2**. Step **6**→**6A** is rather thermoneutral, whereas **6A**→**7** shows increased exothermicity, so that **6**→**7** is thermoneutral for **b** and exothermic for **c** and **d**. Step **7**→**2** is thermoneutral for **b** and endothermic for **c** and **d**. These opposite effects on oxidative addition/reductive elimination by replacement of one CO ligand with a predominantly σ-donating phosphane PR_3[24] can be explained by a general molecular orbital model.[56]

Going from **b** to **d**, the highest barrier is shifted from **5**→**6** to **3**→**4**, with a maximum difference of about 6 kJ mol^{-1} (**c**), and the barriers of **6A**→**7** are lowered by the same amount (**c** and **d**). In contrast to **a**, omission of **6A** does not lead to close approach of the barrier of **6**→**7** to that of **7**→**2**.

Barrier variations correlating with Tolman values are not evident. Thermodynamic trends can be observed for the associations **2**→**3/4**→**5** and the hydrogen addition **6**→**7**: with decreasing Tolman basicity, the exothermicities increase in the former and decrease in the latter case, that is, in the order **d**, **c**, **b** (see Section 3.4.2). For **d**, steric effects apparently exert no influence on thermochemistry or barrier heights.

After zero-point correction, the exothermicities are reduced by up to 10.3 kJ mol^{-1} (**b**, **2**→**3**), and the reaction energies of **6**→**6A** are raised by about 13 kJ mol^{-1}. Consequently, **6**→**6A** is now clearly endothermic for **c** (+ 11.0 kJ mol^{-1}), as is **6**→**7** for **b** (+12.5 kJ mol^{-1}). Other thermodynamic characteristics remain qualitatively unchanged, as does the ranking of the transition states.

Similar to **a**, after free-energy correction **7**→**2** is now the most exergonic reaction, whereas **6**→**6A** shows a strong endergonic shift. Therefore, **6**→**7** becomes endergonic also for **c** and **d**. If one does not consider **6A**, the barrier of **6**→**7** for **b** and **d** is the highest in the catalytic cycle; for **c** it lies above that of **7**→**2**.

System **c′** (phosphane bis-coordination) differs conspicuously from **c** in **6**→**7** and **7**→**2**. Hydrogen addition in **c′** is also—owing to the almost zero barrier of **6A**→**7**—the most

 © 2004 Wiley-VCH Verlag GmbH & Co. KGaA, Weinheim

Table 1. Relative energies [kJ mol^{-1}] of the whole catalytic cycle (see Scheme 2) for systems **a**–**d** at the BP86/TZVP(CE) level with no (first line of each row), zero-point (second line of each row) and free-energy (T = 298.15 K, third line of each row) corrections. For system **a**, additional CCSD(T)//BP86) single-point energies are given after slashes. Values in parentheses belong to single reaction steps; those in italics refer to steps with calculated transition states. Thermodynamic reaction energies are in boldface.

	system **a**	system **b**	system **c**	system **d**	system **c′**
2	0[a]	0[b]	0[c]	0[d]	0[e]
3	−55.8/−80.6	−66.2	−60.1	−56.4	−67.1
	−45.2	−55.9	−51.1	−47.4	−58.0
	+4.5	−19.6	−6.9	+0.2	−9.8
3,4	−8.9 (*46.9*)/−18.5 (*62.1*)	−20.0 (*46.2*)	−5.1 (*55.0*)	−4.0 (*52.4*)	−15.4 (*51.7*)
	−3.7 (*41.5*)	−14.8 (*41.1*)	−0.9 (*50.2*)	−0.1 (*47.3*)	−10.9 (*47.1*)
	+43.4 (*38.9*)	+26.9 (*46.5*)	+44.2 (*51.1*)	+51.2 (*51.0*)	+37.6 (*47.4*)
4	−82.2 (***−26.4***)/−95.1 (***−14.5***)	−81.5 (***−15.3***)	−82.1 (***−22.0***)	−81.3 (***−24.9***)	−83.0 (***−15.9***)
	−64.0 (***−18.8***)	−63.8 (***−7.9***)	−64.8 (***−13.7***)	−62.5 (***−15.1***)	−65.0 (***−7.0***)
	−18.4 (***−22.9***)	−24.5 (***−4.9***)	−23.5 (***−16.6***)	−15.1 (***−15.3***)	−19.0 (***−9.2***)
5	−153.6 (***−71.4***)/−167.0 (***−71.9***)	−173.1 (***−91.6***)	−167.6 (***−85.5***)	−159.8 (***−78.5***)	−176.5 (***−93.5***)
		−147.8 (***−84.0***)	−143.2 (***−78.4***)	−134.3 (***−71.8***)	−152.3 (***−87.3***)
	−128.4 (***−64.4***)	−68.8 (***−44.3***)	−59.4 (***−35.9***)	−47.4 (***−32.3***)	−66.3 (***−47.3***)
	−39.9 (***−21.5***)				
5,6	−102.6 (*51.0*)/−91.5 (*75.5*)	−125.5 (*47.6*)	−118.2 (*49.4*)	−110.4 (*49.4*)	−125.6 (*50.9*)
	−79.3 (*49.1*)	−101.6 (*46.2*)	−95.7 (*47.5*)	−86.4 (*47.9*)	−103.5 (*48.8*)
	+9.3 (*49.2*)	−20.9 (*47.9*)	−10.8 (*48.6*)	+1.7 (*49.1*)	−17.6 (*48.7*)
6	−182.8 (***−29.2***)/−146.0 (***+21.0***)	−186.9 (***−13.8***)	−177.8 (***−10.2***)	−180.0 (***−20.2***)	−184.4 (***−7.9***)
		−158.0 (***−10.2***)	−149.5 (***−6.3***)	−150.8 (***−16.5***)	−156.6 (***−4.3***)
	−153.3 (***−24.9***)	−79.6 (***−10.8***)	−66.8 (***−7.4***)	−65.9 (***−18.5***)	−72.0 (***−5.7***)
	−66.0 (***−26.1***)				
6A	−168.2 (***+14.6***)/−147.5 (***−1.5***)	−181.1 (***+5.8***)	−180.2 (***−2.4***)	−176.5 (***+3.5***)	−192.9 (***−8.5***)
		−139.5 (***+18.5***)	−138.5 (***+11.0***)	−134.7 (***+16.1***)	−150.9 (***+5.7***)
	−128.1 (***+25.2***)	−32.0 (***+47.6***)	−24.6 (***+42.2***)	−18.1 (***+47.8***)	−35.0 (***+37.0***)
	−11.8 (***+54.2***)				
6A,7[f]	−149.7 (*18.5*)/−134.6 (*11.4*)	−168.9 (*12.2*)	−173.7 (*6.5*)	−170.0 (*6.5*)	−190.1 (*2.8*)
	−112.5 (*15.6*)	−131.8 (*7.7*)	−136.1 (*2.4*)	−132.0 (*2.7*)	−152.1 (*−1.2*)
	+2.9 (*14.7*)	−22.7 (*9.3*)	−20.2 (*4.4*)	−13.7 (*4.4*)	−34.4 (*0.6*)
7	−172.9 (***−4.7***)/−162.7 (***−16.7***)	−189.6 (***−8.5***)	−199.4 (***−19.2***)	−200.6 (***−24.1***)	−219.1 (***−26.2***)
		−145.5 (***−6.0***)	−154.4 (***−15.9***)	−155.5 (***−20.8***)	−174.0 (***−23.1***)
	−128.8 (***−0.7***)	−35.3 (***−3.3***)	−37.8 (***−13.2***)	−36.1 (***−18.0***)	−58.9 (***−23.9***)
	−11.7 (***+0.1***)				
7,2	−138.3 (*34.6*)/−118.1 (*44.6*)	−151.0 (*38.6*)	−160.2 (*39.2*)	−165.3 (*35.3*)	−176.7 (*42.4*)
	−98.2 (*30.6*)	−110.6 (*34.9*)	−119.4 (*35.0*)	−123.8 (*31.7*)	−134.7 (*39.3*)
	+19.5 (*31.2*)	+0.1 (*35.2*)	−3.6 (*34.2*)	−3.7 (*32.4*)	−17.3 (*41.6*)
2	−190.2 (***−17.3***)/−153.0 (***+9.7***)	−190.2 (***−0.6***)	−190.2 (***+9.2***)	−190.2 (***+10.4***)	−190.2 (***+28.9***)
		−144.7 (***+0.8***)	−144.7 (***+9.7***)	−144.7 (***+10.8***)	−144.7 (***+29.3***)
	−144.7 (***−15.9***)	−81.4 (***−46.1***)	−81.4 (***−43.6***)	−81.4 (***−45.3***)	−81.4 (***−22.5***)
	−81.4 (*−69.7*)				

[a] Reference is **2-CO** (see Section 3.3.1 and Figure 1). [b] Reference is **2-PF$_3$-*t*** (see Section 3.3.1 and Figure 1). [c] Reference is **2-PH$_3$-*t*** (see Section 3.3.1 and Figure 1). [d] Reference is **2-PMe$_3$-*t*** (see Section 3.3.1 and Figure 1). [e] Reference is **2-(PH$_3$)$_2$-*ct*** (see Section 3.3.1 and Figure 1). [f] Barrier values relative to **6A**.

favourable for all systems studied here. On the other hand, **7**→**2** for **c′** has the highest endothermicity and the highest barrier (cf. above). Barriers for **3**→**4**, **5**→**6** and **6A**→**7** merge with their counterparts in **c** to within 5 kJ mol^{-1}; the values of the first two are nearly identical.

Relative to **2**, all energies of **c′** versus **c** are lower, with a maximum difference of −19.7 kJ mol^{-1} for intermediate **7**. Note, however, that **2-(PH$_3$)$_2$-*ct*** is destabilised versus **2-PH$_3$-*t*** by +49.0 kJ mol^{-1} (cf. Section 3.2 and Scheme 3). A possible transition from **c** to **c′**, as chosen by Morokuma et al.,[12] **4-PH$_3$-*c*** + **PH$_3$**→**5-(PH$_3$)$_2$-*ee*** (see Figure 1), recoups −45.4 kJ mol^{-1}, but the CO addition within **c**, **4-PH$_3$-*c*** + **CO**→**5-(PH$_3$)$_2$-*e*** (see Figure 1), gives −85.5 kJ mol^{-1}. Though these gaps between **c′** and **c** move together for ligands other than PH$_3$ (cf. Section 3.2), industrial CO pressures of more than 1 MPa[1a] should support phosphane monocoordination.

With inclusion of zero-point and free-energy corrections the trends are similar to system **c** (cf. above).

3.3.3. Connections to experimental observations and former calculations: The deviating profiles for **6**→**7** explain why the rate of the unmodified system **a** responds positively (in first order) towards hydrogen pressure,[57] whereas the influence of hydrogen on modified catalysts becomes zero with increasing phosphane concentration,[46] that is, supersession of in situ generated unmodified species in favour of phosphane mono- or even bis-coordination (cf. Section 3.1).

Inhibiting effects of high CO pressure and/or phosphane concentration can be attributed to the exothermic associations **2**→**1** (trapping of the active species) or **6**→**9** (see Scheme 2).[2,46] Furthermore, in addition to the instability of [HRh(CO)$_4$] towards cluster formation (cf. Section 3.1), for **a** the combination of an exothermic and unhindered reac-

© 2004 Wiley-VCH Verlag GmbH & Co. KGaA, Weinheim

Table 2. Relative energies [kJ mol^{-1}] of **2**→**3/3**→**4** for the alternative active species **2-PR$_3$-*c*/2-(PH$_3$)$_2$-*cc*** of systems **b**–**d** on the BP86/TZVP(CE) level with no (first line of each row), zero-point (second line of each row), and free energy (T = 298.15 K, third line of each row) corrections (see also Table 1).

	system **a**	system **b**	system **c**	system **d**	system **c′**
2	0[a]	+0.0[b]	−4.9[c]	−10.0[d]	−7.8[e]
		+0.0[b]	−4.5[c]	−9.9[d]	−6.2 [e]
		−7.5[b]	−3.6[c]	−8.6[d]	−2.9[e]
3	−55.8	−75.5 (***−75.5***)	−62.2 (***−57.3***)	−57.0 (***−47.0***)	−68.0 (***−60.2***)
	−45.2	−64.8 (***−64.8***)	−52.5 (***−48.0***)	−47.3 (***−37.4***)	−57.5 (***−51.3***)
	+4.5	−23.3 (***−15.8***)	−7.1 (***−3.5***)	+1.4 (***+7.2***)	−9.0 (***−6.1***)
3,4	−8.9 (*46.9*)	−35.2 (*40.3*)	−16.2 (*46.0*)	−1.5 (*55.5*)	−13.6 (*54.4*)
	−3.7 (*41.5*)	−29.3 (*35.5*)	−11.9 (*40.6*)	+3.8 (*51.1*)	−8.8 (*48.7*)
	+43.4 (*38.9*)	+12.1 (*35.4*)	+33.7 (*40.8*)	+50.0 (*51.4*)	+39.4 (*48.4*)
4	−82.2 (***−26.4***)	−81.5 (***−6.0***)	−82.1 (***−19.9***)	−81.3 (***−24.3***)	−71.1 (***−3.1***)
	−64.0 (***−18.8***)	−63.8 (***+1.0***)	−64.8 (***−12.3***)	−62.5 (***−15.2***)	−55.4 (***+2.1***)
	−18.4 (***−22.9***)	−24.5 (***−1.2***)	−23.5 (***−16.4***)	−15.1 (***−16.5***)	−11.9 (***−2.9***)

[a] Reference is **2-CO** (see Section 3.3.1 and Figure 1). [b] Reference is **2-PF$_3$-*t*** (see Section 3.3.1 and Figure 1). [c] Reference is **2-PH$_3$-*t*** (see Section 3.3.1 and Figure 1). [d] Reference is **2-PMe$_3$-*t*** (see Section 3.3.1 and Figure 1). [e] Reference is **2-(PH$_3$)$_2$-*ct*** (see Section 3.3.1 and Figure 1).

tion **6**→**9**[58] with the endothermic and rather hindered hydrogen addition **6**→**7** (cf. above) may be the reason why **9** and not **1** (see Scheme 2) is the resting state during catalysis.[57]

For all systems **6A**→**7** has the lowest calculated barrier in the cycle (2.8 (**c′**) to 18.5 kJ mol^{-1} (**a**) at the uncorrected BP86/TZVP(CE) level). Neglecting **6A**, the position of the hydrogen-addition barrier changes markedly after free-energy correction, but the qualitative differences between the systems remain constant (cf. above). The next in rank is **7**→**2** [35.3 (**d**) to 44.6 kJ mol^{-1} (**a**)], while the barriers of insertions **3**→**4/5**→**6** jointly amount to values of around 50 kJ mol^{-1}. This order was already found in previous theoretical studies,[12,17a] but the experimentally disproved assumption that step **6**→**7** is always rate-determining[2,46,59,60] was defended in terms of possible solvent coordination to **6**. However, interactions of this kind could not be detected spectroscopically.[46] An ethene adduct of the unmodified complex **6**, C_2H_4 + **6**→[$C_3H_5ORh(CO)_3(C_2H_4)$], was postulated recently.[61] There may be a connection to the kinetics of ethene saturation or even inhibition at very low phosphane concentrations.[46] For more relevant higher phosphane concentrations the rate dependence on ethene is first-order.[46] Since increasing CO pressure then lowers the catalytic turnover (cf. above), CO insertion **5**→**6** has been ruled out as rate-determining in favour of ethene association/insertion **2**→**3/3**→**4**.[46] It must be stressed, however, that "hydroformylation reactions are extremely sensitive to experimental conditions".[2] The model character of our systems thus prevents an unequivocal statement about the step with the highest reaction barrier. Nevertheless, we agree with mechanistic studies that the activity race should be mainly decided *before* hydrogen addition **6**→**7**.

3.4. Early catalytic steps: The catalytic cycle as a whole does not give a clear picture about activity differences between the systems. Especially the presumed better performances of unmodified system **a** and system **b** with the least basic phosphane ligand (cf. Introduction) are still obscure. With regard to the discussion in Section 3.3.2 we now take a closer look at the first two steps, ethene association/insertion **2**→**3/3**→**4**. This is also justified by the fact that insertion of higher olefins into the rhodium–hydride bond has proven to be decisive for hydroformylation selectivity (see Scheme 1).[2,4–9,16,17]

3.4.1. Ethene insertion: Energies with the alternative active species **2-PR$_3$-*c*/2-(PH$_3$)$_2$-*cc*** (cf. Section 3.3.1) are listed in Table 2.

The exothermicities of **3**→**4** for **b**, **c** and **c′** are less pronounced than for **2-PR$_3$-*t*/2-(PH$_3$)$_2$-*ct*** (see Table 1). Thus, to an even greater extent **b** gains the lowest and **a** the highest value. In contrast to **2-PR$_3$-*t*/2-(PH$_3$)$_2$-*ct***, the barriers for **b**, **c** and **d** increase with increasing Tolman basicity. The values for **b** and **c** are lower by up to 10 kJ mol^{-1}, and those for **d** and **c′** increase by less than 5 kJ mol^{-1}. System **a** now reaches only the barrier level of **c**, while in the case of **2-PR$_3$-*t*/2-(PH$_3$)$_2$-*ct*** the lowest value was shared by **a** and **b**. Ethene insertion therefore offers thermodynamic advantages for **a**, but kinetic preferences for **b**.

3.4.2. Ethene association: The stabilisation of **2-PR$_3$-*c*/2-(PH$_3$)$_2$-*cc*** versus **2-PR$_3$-*t*/2-(PH$_3$)$_2$-*ct*** (up to −10.0 kJ mol^{-1}, see first row of Table 2) is for **c** and **d** nearly compensated by the lower exothermicities of **2**→**3** (see second row of Table 1 and Table 2, respectively).

Free-energy correction reduces the exothermicities drastically. For **2-CO** and **2-PMe$_3$-*c*/*t*** the association even becomes thermoneutral or weakly endothermic. However, the ranking for **2-PR$_3$** (beginning with the lowest exothermicity) remains qualitatively almost the same; for **2-PR$_3$-*c*** it is $PMe_3 \approx CO < PH_3 \ll PF_3$, and for **2-PR$_3$-*t*** $CO \approx PMe_3 < PH_3 \ll PF_3$.[54] Decreasing Tolman basicity is therefore expected to make olefin association more exothermic, which, together with the partially decreasing barriers of **3**→**4** (cf. Section 3.4.1), may rationalise the higher activity of systems with less basic phosphanes. Unfortunately, this argumentation cannot explain the outstandingly high activity of **a**, for, in spite of a moderate subsequent insertion barrier (cf. Section 3.4.1), the association energy of **2-CO** is comparatively unfavourable. A similar dilemma is posed by the low activity of systems with two monophosphane ligands or chelates:[2]

 © 2004 Wiley-VCH Verlag GmbH & Co. KGaA, Weinheim

although the ethene-insertion barriers of the model system **c′** are rather high (see Tables 1 and 2), the association energy of **2-$(PH_3)_2$-*ct*** is similar to that of **2-PF_3-*t***, and in the case of **2-$(PH_3)_2$-*cc*** it is comparable to that of **2-PH_3-*c***.

Since substrate capture is indispensable for catalysis, the question arises whether the catalytic activity is controlled by reaction barriers of **2**→**3**, the more so as the olefin concentration is low under normal experimental conditions.[46] The only published transition states **2,3** belong to systems with a chelating bis-phosphane ligand and have been reported without geometry information.[18] To obtain a first overview of the potential energy surface we performed a series of 0.3 ps CPMD simulations under NVE conditions. The starting geometries are depicted in Scheme 4.

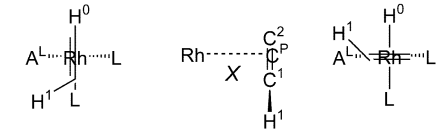

Scheme 4. Starting geometries for CPMD simulations of the olefin association **2**→**3**.

Ethene was arranged parallel (***p***) or vertical (***v***) with respect to the rhodium–hydride bond of **2** (further geometrical parameters are given in Scheme 4). The initial distance X between Rh and the pseudoatom C^P was set to 3.0 and 3.5 Å, respectively, and the starting temperature was $T=0$ K. These unified "reaction conditions" are rather far from experiment, but they give hints on the capability of **2** for substrate capture: ethene will either associate (+) or move away (−) (Table 3).

In five isomers—**2-PH_3-*c***, **2-PMe_3-*c***, **2-PMe_3-*t***, **2-$(PH_3)_2$-*ct*** and **2-$(PH_3)_2$-*cc***—association is apparently hindered. Static transition-state searches for **2,3** indeed converged only in these cases.[62] The transition-state geometries are essentially similar and nearer to the ***v*** arrangement (Table 4 and Figure 4).

The distance X lies between 3.27 (**2,3-$(PH_3)_2$-*cc***) and 3.57 Å (**2,3-PH_3-*c***), and C^1-C^P-Rh-H^0 ranges from +62.45° (**2,3-PMe_3-*t***) to +73.14° (**2,3-$(PH_3)_2$-*ct***). H^1-C^1-C^P-Rh deviates for the latter two transition states significantly from −90°, that is, ethene is tilted with respect to the Rh–H^0 bond.

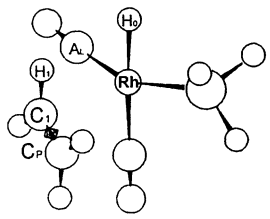

Figure 4. Structure of the localised transition state **2,3-PH_3-*c*** (see Scheme 4 and Table 4).

Table 3. Positive (+) or negative (−) olefin association tendencies in reaction **2**→**3** during 0.3 ps CPMD simulations under NVE conditions (see Scheme 4 and text).

R	**2-CO**→ **3-CO**[a]	**2-PR_3-*c***→ **3-PR_3-*e***[a]	**2-PR_3-*t***→ **3-PR_3-*a***[a]	**2-$(PR_3)_2$-*ct***→ **3-$(PR_3)_2$-*ae***[a]	**2-$(PR_3)_2$-*cc***→ **3-$(PR_3)_2$-*ee***[a]
– (**a**)	3.0 Å/***p*** (+) 3.0 Å/***v*** (+) 3.5 Å/***p*** (+) 3.5 Å/***v*** (+)	–	–	–	–
F (**b**)	–	3.0 Å/***p*** (+) 3.0 Å/***v*** (+) 3.5 Å/***p*** (+) 3.5 Å/***v*** (+)	3.0 Å/***p*** (+) 3.0 Å/***v*** (+) 3.5 Å/***p*** (+) 3.5 Å/***v*** (+)	–	–
H (**c**)	–	3.0 Å/***p*** (+) 3.0 Å/***v*** (+) 3.5 Å/***p*** (−) 3.5 Å/***v*** (−)	3.0 Å/***p*** (+) 3.0 Å/***v*** (+) 3.5 Å/***p*** (+) 3.5 Å/***v*** (+)	3.0 Å/***p*** (+) 3.0 Å/***v*** (−) 3.5 Å/***p*** (−) 3.5 Å/***v*** (−)	3.0 Å/***p*** (+) 3.0 Å/***v*** (+) 3.5 Å/***p*** (−) 3.5 Å/***v*** (−)
Me (**d**)	–	3.0 Å/***p*** (−) 3.0 Å/***v*** (−) 3.5 Å/***p*** (−) 3.5 Å/***v*** (−)	3.0 Å/***p*** (−) 3.0 Å/***v*** (+) 3.5 Å/***p*** (−) 3.5 Å/***v*** (−)	–	–

[a] See Section 3.3.1 and Figure 1.

Table 4. Energies E [kJ mol^{-1}] and geometrical parameters (see Scheme 4 and Figure 4) for the localised transition states **2,3**.

	2,3-PH_3-*c*	**2,3-PMe_3-*c***	**2,3-PMe_3-*t***	**2,3-$(PH_3)_2$-*ct***	**2,3-$(PH_3)_2$-*cc***
E[a]	+0.4 +2.2 +35.2	+3.4 +5.6 +42.4	−5.1 −2.8 +34.9	+0.4 +1.8 +35.8	+5.7 +7.6 +42.7
X [Å]	3.57	3.34	3.49	3.51	3.27
C^1-C^P-Rh	57.42	60.12	54.91	55.15	64.46
C^P-Rh-H^0	91.32	93.14	91.78	93.19	91.19
C^P-Rh-A^L	108.77	104.77	112.39	111.74	105.70
H^1-C^1-C^P-Rh	−98.19	−95.63	−51.86	−65.23	−92.58
C^1-C^P-Rh-H^0	+63.49	+68.42	+62.45	+73.14	+67.10

[a] BP86/TZVP(CE) level with no (first line), zero-point (second line) and free-energy ($T=298.15$ K, third line) corrections.

Transition-state energies in Table 4 are almost exclusively composed of entropic contributions. Steric strain seems to raise them if one compares the values of **2,3-PMe_3-*c*** versus **2,3-PMe_3-*t***, **2,3-$(PH_3)_2$-*cc*** versus **2,3-$(PH_3)_2$-*ct*** or the ener-

© 2004 Wiley-VCH Verlag GmbH & Co. KGaA, Weinheim

gies for the bis-phosphane systems (ca. 20 kJ mol^{-1} before and 80 kJ mol^{-1} after free energy correction).[18] One could argue that steric bulk is exclusively responsible for the barriers, but there must be also an influence of electronic factors, as is demonstrated by the apparent lack of **2,3-PF$_3$-*c***. In the case of real-size phosphane ligands, however, **2,3** should always exist.

Taking into account transition states for ethene association gives the only consistent explanation for expected activity differences: The performance of **a** is then chiefly the consequence of unhindered olefin association, while phosphane-modified systems suffer from association barriers which depend on the steric demand (modelled by **d** and **c′**), and for ligands with similar size but variable Tolman basicity (substituted arylphosphanes, modelled by **b** and **c**) the thermochemistry is decisive.

4. Conclusion

Static and dynamic quantum-mechanical approaches at different levels of theory allow several valuable statements to be made regarding the catalytic activity of four rhodium hydroformylation sytems **a**–**d**, distinguished by phosphane modification and corresponding phosphane (Tolman) basicity:

1) In agreement with mechanistic studies, phosphane monocoordination in systems **b**–**d** is estimated to be predominant during catalysis.
2) The greater sensitivity of the unmodified system **a** towards hydrogen pressure and its different resting state can be explained by a less favourable energy profile of hydrogen addition **6**→**7**. Although the model character of our systems prevents an unequivocal statement about the step with the highest reaction barrier, the experimentally disproved assumption that **6**→**7** is always rate-determining is also questioned by our calculations. CO/olefin insertions **5**→**6**/**3**→**4** are favoured instead, and the preference of early catalytic steps matches conclusions drawn from experiment.
3) Neither the catalytic cycle as a whole nor olefin insertion **3**→**4** as an important selectivity-determining step gives a clear picture about activity differences among systems **a**–**d**. Yet if one focuses the activity discussion on the crucial first catalytic step, olefin association **2**→**3**, new light is thrown on the experimentally observed higher activity of **a** and systems with less basic phosphane ligands, modelled by **b**. For **a**, no transition state **2,3** could be found by a combination of dynamic and static calculations, and the association is barrierless. On the other hand, transition states should always exist for systems modified by real-size phosphane ligands, that is, the substrate will sometimes not be captured and move away, which hampers the catalytic activity. Olefin association concurrently becomes thermodynamically more favoured with decreasing Tolman basicity, that is, in the order **d**, **c**, **b**. The catalytic performance thus depends on a subtle interplay of kinetic and thermodynamic factors.

Acknowledgments

We thank the ZI of the University of Zurich and the CSCS in Manno for generous support. D.G. also thanks the German Science Foundation for a research grant.

[1] a) B. Cornils in *Catalysis from A to Z* (Eds.: B. Cornils, W. A. Herrmann, R. Schlögl, H.-C. Wong), Wiley-VCH, Weinheim, **2000**, pp. 279–281; b) M. Beller, B. Cornils, C. D. Frohning, C. W. Kohlpaintner, *J. Mol. Catal. A* **1995**, *104*, 17–85; c) B. Cornils in *New Syntheses with Carbon Monoxide* (Ed.: J. Falbe), Springer, New York, **1980**, pp. 1–225.
[2] P. W. N. M. van Leeuwen, C. P. Casey, G. T. Whiteker in *Rhodium Catalyzed Hydroformylation* (Eds.: P. W. N. M. van Leeuwen, C. Claver), Kluwer Academic Publishers, Dordrecht, **2000**, pp. 63–106.
[3] M. Torrent, M. Solà, G. Frenking, *Chem. Rev.* **2000**, *100*, 439–493.
[4] D. Gleich, R. Schmid, W. A. Herrmann, *Organometallics* **1998**, *17*, 4828–4834.
[5] W. R. Rocha, W. B. de Almeida, *Int. J. Quantum Chem.* **2000**, *78*, 42–51.
[6] J. J. Carbó, F. Maseras, C. Bo, P. W. N. M. van Leeuwen, *J. Am. Chem. Soc.* **2001**, *123*, 7630–7637.
[7] S. A. Decker, T. A. Cundari, *J. Organomet. Chem.* **2001**, *635*, 132–141.
[8] G. Alagona, C. Ghio, R. Lazzaroni, R. Settambolo, *Organometallics* **2001**, *20*, 5394–5404.
[9] a) D. Gleich, R. Schmid, W. A. Herrmann, *Organometallics* **1998**, *17*, 2141–2143; b) D. Gleich, W. A. Herrmann, *Organometallics* **1999**, *18*, 4354–4361.
[10] a) R. Paciello, L. Siggel, M. Röper, *Angew. Chem.* **1999**, *111*, 2045–2048; *Angew. Chem. Int. Ed.* **1999**, *38*, 1920–1921; b) R. Paciello, L. Siggel, H.-J. Kneuper, N. Walker, M. Röper, *J. Mol. Catal. A* **1999**, *143*, 85–97.
[11] R. Schmid, W. A. Herrmann, G. Frenking, *Organometallics* **1997**, *16*, 701–708.
[12] T. Matsubara, N. Koga, Y. Ding, D. G. Musaev, K. Morokuma, *Organometallics* **1997**, *16*, 1065–1078.
[13] A. D. Becke, *Phys. Rev. A* **1988**, *38*, 3098–3100.
[14] C. Lee, W. Yang, R. G. Parr, *Phys. Rev. B* **1988**, *37*, 785–789.
[15] A. D. Becke, *J. Chem. Phys.* **1993**, *98*, 1372–1377.
[16] a) D. Gleich in *Applied Homogeneous Catalysis with Organometallic Compounds, Vol. 2* (Eds.: B. Cornils, W. A. Herrmann), Wiley-VCH, Weinheim, **2002**, pp. 727–737; b) D. Gleich, PhD thesis, Technical University of Munich (Germany), **1999**.
[17] a) S. A. Decker, T. R. Cundari, *Organometallics* **2001**, *20*, 2827–2841; b) S. A. Decker, T. R. Cundari, *New J. Chem.* **2002**, *26*, 129–135.
[18] C. R. Landis, J. Uddin, *J. Chem. Soc. Dalton Trans.* **2002**, 729–742.
[19] M. Svensson, S. Humbel, R. D. J. Fröse, T. Matsubara, S. Sieber, K. Morokuma, *J. Phys. Chem.* **1996**, *100*, 19357–19363.
[20] D. Bakowies, W. Thiel, *J. Phys. Chem.* **1996**, *100*, 10580–10594.
[21] U. Pidun, G. Frenking, *Chem. Eur. J.* **1998**, *4*, 522–540.
[22] R. J. Bartlett, *J. Phys. Chem.* **1989**, *93*, 1697–1708.
[23] a) C. A. Tolman, *Chem. Rev.* **1977**, *77*, 313–348; b) C. A. Tolman, *J. Am. Chem. Soc.* **1970**, *92*, 2953–2956.
[24] G. Frenking, K. Wichmann, N. Fröhlich, J. Grobe, W. Golla, D. Le Van, B. Krebs, M. Läge, *Organometallics* **2002**, *21*, 2921–2930.
[25] C. R. Landis, S. Feldgus, J. Uddin, C. E. Wozniak, *Organometallics* **2000**, *19*, 4878–4886.
[26] a) R. Car, M. Parrinello, *Phys. Rev. Lett.* **1985**, *55*, 2471–2474; b) D. Marx, J. Hutter in *Modern Methods and Algorithms of Quantum Chemistry* (Ed.: J. Grotendorst), NIC Series, Jülich, **2000**, Vol. 1, pp. 301–449.
[27] M. Cheong, R. Schmid, T. Ziegler, *Organometallics* **2000**, *19*, 1973–1982.
[28] P. Margl, T. Ziegler, P. E. Blöchl, *J. Am. Chem. Soc.* **1995**, *117*, 12625–12634.
[29] H. M. Senn, P. E. Blöchl, A. Togni, *J. Am. Chem. Soc.* **2000**, *122*, 4098–4107.

 © 2004 Wiley-VCH Verlag GmbH & Co. KGaA, Weinheim

[30] O. M. Aagaard, R. J. Meier, F. Buda, *J. Am. Chem. Soc.* **1998**, *120*, 7174–7182.
[31] B. B. Coussens, F. Buda, H. Oevering, R. J. Meier, *Organometallics* **1998**, *17*, 795–801.
[32] Gaussian 98, Revision A.5, M. J. Frisch, G. W. Trucks, H. B. Schlegel, G. E. Scuseria, M. A. Robb, J. R. Cheeseman, V. G. Zakrzewski, J. A. Montgomery, Jr., R. E. Stratmann, J. C. Burant, S. Dapprich, J. M. Millam, A. D. Daniels, K. N. Kudin, M. C. Strain, O. Farkas, J. Tomasi, V. Barone, M. Cossi, R. Cammi, B. Mennucci, C. Pomelli, C. Adamo, S. Clifford, J. Ochterski, G. A. Petersson, P. Y. Ayala, Q. Cui, K. Morokuma, D. K. Malick, A. D. Rabuck, K. Raghavachari, J. B. Foresman, J. Cioslowski, J. V. Ortiz, B. B. Stefanov, G. Liu, A. Liashenko, P. Piskorz, I. Komaromi, R. Gomperts, R. L. Martin, D. J. Fox, T. Keith, M. A. Al-Laham, C. Y. Peng, A. Nanayakkara, C. Gonzalez, M. Challacombe, P. M. W. Gill, B. Johnson, W. Chen, M. W. Wong, J. L. Andres, C. Gonzalez, M. Head-Gordon, E. S. Replogle, J. A. Pople, Gaussian Inc., Pittsburgh, PA, **1998**.
[33] N. Godbout, D. R. Salahub, J. Andzelm, E. Wimmer, *Can. J. Chem.* **1992**, *70*, 560–571.
[34] R. B. Ross, J. M. Powers, T. Atashroo, W. C. Ermler, L. A. LaJohn, P. A. Christiansen, *J. Chem. Phys.* **1990**, *93*, 2812–2824.
[35] J. P. Perdew, *Phys. Rev. B* **1986**, *33*, 8822–8824.
[36] D. Gleich, J. Hutter, unpublished results.
[37] CPMD V3.7, Copyright IBM Corp., **1990–2003**, MPI für Festkörperforschung Stuttgart, **1997–2001**.
[38] C. Hartwigsen, S. Goedecker, J. Hutter, *Phys. Rev. B* **1998**, *58*, 3641–3662.
[39] W. G. Hoover, *Phys. Rev. A* **1985**, *31*, 1695–1697.
[40] P. E. Blöchl, H. M. Senn, A. Togni in *Transition State Modeling for Catalysis* (Eds.: D. G. Truhlar, K. Morokuma), American Chemical Society, Washington, **1999**, pp. 88–99.
[41] a) C. K. Brown, G. Wilkinson, *J. Chem. Soc. A* **1970**, 2753–2764; b) D. Evans, J. A. Osborn, G. Wilkinson, *J. Chem. Soc. A* **1968**, 3133–3142.
[42] R. F. Heck, D. S. Breslow, *J. Am. Chem. Soc.* **1961**, *83*, 4023–4027.
[43] C. Li, E. Widjaja, W. Chew, M. Garland, *Angew. Chem.* **2002**, *114*, 3940–3943; *Angew. Chem. Int. Ed.* **2002**, *41*, 3785–3789.
[44] N. N. Greenwood, A. Earnshaw, *Chemistry of the Elements*, Butterworth-Heinemann, Oxford, **1997**, p. 1134.
[45] L. A. van der Veen, P. H. Keven, G. C. Schoemaker, J. N. H. Reek, P. C. J. Kamer, P. W. N. M. van Leeuwen, M. Lutz, A. Spek, *Organometallics* **2000**, *19*, 872–883.
[46] G. Kiss, E. J. Mozeleski, K. C. Nadler, E. VanDriessche, C. DeRoover, *J. Mol. Catal. A* **1999**, *138*, 155–176.
[47] C. Møller, M. S. Plesset, *Phys. Rev.* **1934**, *46*, 618.
[48] Our nomenclature for phosphane-coordinated rhodium complexes gives the numbering according to Scheme 2, then the type and number of phosphane ligands, and finally the phosphane arrangement. Relative to rhodium–hydride, –alkyl, and –acyl bonds, the arrangement for pentacoordinated complexes is axial (***a***) and/or equatorial (***e***), and in the case of tetracoordination it is *cis* (***c***) and/or *trans* (***t***).
[49] D. L. Thorn, R. Hoffmann, *J. Am. Chem. Soc.* **1978**, *100*, 2079–2090.
[50] M. J. Burk, M. P. McGrath, R. Wheeler, R. H. Crabtree, *J. Am. Chem. Soc.* **1988**, *110*, 5034–5039.
[51] F. Abu-Hasanayn, K. Krogh-Jespersen, A. S. Goldman, *J. Am. Chem. Soc.* **1994**, *116*, 5979–5980.
[52] M. A. Esteruelas, L. A. Oro, *Chem. Rev.* **1998**, *98*, 577–588.
[53] F. Maseras, A. Lledós, M. Costas, J. M. Poblet, *Organometallics* **1996**, *15*, 2947–2953.
[54] An energy difference of less than 5 kJ mol^{-1} lies within the so-called chemical accuracy. We chose "$<$" as notation for differences of 5–10 kJ mol^{-1}, "$\ll$" for 10–15 kJ mol^{-1}, and "$\ll<$" for more than 15 kJ mol^{-1}.
[55] T. K. Dargel, R. H. Hertwig, W. Koch, *J. Chem. Phys.* **1998**, *108*, 3876–3885.
[56] J.-Y. Saillard, R. Hoffmann, *J. Am. Chem. Soc.* **1984**, *106*, 2006–2026.
[57] a) J. Feng, M. Garland, *Organometallics* **1999**, *18*, 417–424; b) G. Liu, R. Volken, M. Garland, *Organometallics* **1999**, *18*, 3429–3436.
[58] CO associations are assumed to be barrierless (cf. Section 3.2). **6**→**9** is exothermic for **a** with −58.3 kJ mol^{-1} at the uncorrected BP86/TZVP(CE) level.
[59] S. C. van der Slot, P. C. J. Kamer, P. W. N. M. van Leeuwen, J. A. Iggo, B. T. Heaton, *Organometallics* **2001**, *20*, 430–441.
[60] K. Nozaki, T. Matsuo, F. Shibahara, T. Himaya, *Organometallics* **2003**, *22*, 594–600.
[61] J. Zhang, M. Poliakoff, M. W. George, *Organometallics* **2003**, *22*, 1612–1618.
[62] Starting structures for optimisations with Gaussian 98 (partially reduced step size) were taken from trajectory snapshots after 0.1 ps. Transition states are characterised by one imaginary frequency below 100 cm^{-1} (similar to ref. [18]) and appropriate eigenvectors.

Received: May 26, 2003
Revised: December 22, 2003 [F5179]

Published online: March 12, 2004

© 2004 Wiley-VCH Verlag GmbH & Co. KGaA, Weinheim